Received: 15 November 2016 | Revised: 3 July 2017 | Accepted: 15 July 2017

DOI: 10.1111/ffe.12690

ORIGINAL CONTRIBUTION

WILEY

Fatigue crack propagation under in-phase and out-of-phase biaxial loading

R.K. Neerukatti[1] | S. Datta[1] | A. Chattopadhyay[1] | N. Iyyer[2] | N. Phan[3]

[1]Arizona State University, Tempe, AZ 85287, USA

[2]Technical Data Analysis, Inc, Falls Church, VA 22042, USA

[3]US Naval Air Systems Command, Patuxent River, MD 20670, USA

Correspondence
R. K. Neerukatti, Arizona State University, Tempe, AZ 85287, USA.
Email: rajesh.neerukatti@asu.edu

Funding information
U.S. Naval Air Systems Command and Technical Data Analysis Inc., Grant/Award Number: N08-006 Phase III DO 0005; US Navy Naval Air Systems Command

Abstract

Fatigue damage characteristics of aluminium alloy under complex biaxial loads such as in-phase and out-of-phase loading conditions and different biaxiality ratios have been investigated. The effects of microscale phenomena on macroscale crack growth were studied to develop an in-depth understanding of crack nucleation and growth. Material characterization was conducted to study the microstructure variability. Scanning electron microscopy was used to identify the second phase particles, and energy dispersive X-ray spectroscopy was performed to analyse their phases and elements. Extensive quasi-static and fatigue tests were conducted on Al7075-T651 cruciform specimens over a wide range of load ratios and phases. Detailed fractography analysis was conducted to understand the crack growth behaviour observed during the fatigue tests. Significant differences in crack initiation and propagation behaviour were observed when a phase difference was applied. Primarily, crack retardation and splitting were observed because of the constantly varying mode mixity caused by phase difference. The crack growth behaviour and fatigue lives under out-of-phase loading were compared with those under in-phase loading to understand the effect of mixed-mode fracture.

KEYWORDS

aluminium alloy 7075, biaxial fatigue, fatigue crack propagation, fractography, in-phase and out-of-phase loading

1 | INTRODUCTION

Metallic aerospace components are generally subjected to complex multiaxial loading such as a combination of biaxial proportional, nonproportional, in-phase, and out-of-phase loading conditions.[1-3] Although extensive studies have been conducted to understand their fatigue characteristics under uniaxial (constant and variable amplitude) loading, very few studies have been reported on the effects of multiaxial loading conditions on crack initiation and propagation.[4-8] The time to failure depends on a multitude of variables, many of which are stochastic in nature. Some of the variables include "usage" history, defect geometry and location, material used, and applied load characteristics. While recent studies have shown the effects of property variability and defects at the microstructural level on crack initiation, manifestations of microstructural characteristics in macroscale phenomena under complex loading have not been adequately investigated.

Under biaxial loading, the initiation and propagation of cracks depend on a number of factors such as load biaxiality ratio, phase difference, and proportionality. Several theories have been proposed to predict the small

Nomenclature: K_I, = Mode I stress intensity factor; K_{II}, = Mode II stress intensity factor; M_R, = Mode-mixity ratio; θ, = Angle of crack propagation

crack initiation under mixed-mode loading based on stress-strain, energy, and critical plane approaches.[9-11] A crystal plasticity micromechanical model embedded with finite elements was developed by Bennett and McDowell[12] and Zhang et al[13] to assess the effect of grain orientations on the crack initiation behaviour. Zhang et al[13] developed a physics-based multiscale damage criterion to predict the fatigue crack initiation life under in-plane biaxial Fighter Aircraft Loading STandard For Fatigue (FALSTAFF) loading. However, the crack propagation under different types of in-plane biaxial loading has not yet been completely studied and therefore, is the focus of this paper.

The crack growth under mixed-mode loading is significantly different from that of uniaxial loading (where K_I is the primary crack driving force), and different theories have been proposed to predict the crack propagation. Erdogan and Sih[14] proposed a hypothesis for mixed-mode fracture on the basis of the maximum tangential stress criterion and postulated that the crack under mixed-mode loading extends in the direction perpendicular to the maximum tangential stress (under elastic conditions) ahead of the crack tip. Sih[15] proposed that the crack extends in the direction of minimum strain energy density. The maximum tangential stress and minimum strain energy criteria predict similar crack propagation directions and are applicable to the Paris crack growth regime. Hallback and Nilsson[16] proposed that the cracks propagate in a direction collinear with the plane of maximum shear stress rather than propagating perpendicular to the plane of maximum tangential stress. This model is valid for unstable crack growth in microstructurally small cracks and under severe plastic deformation under torsion. It is important to note that these models were developed on the basis of either axial-torsion loading or by applying intermediate mode II loads on mode I fatigue loading. A limited amount of research has been reported on the material behaviour under in-plane biaxial loads.[3] Hopper and Miller[2] studied fatigue crack propagation in biaxially stressed notched and unnotched plates and found that the rate of crack propagation is affected by the biaxial stress state near the crack tip. Anderson and Garret[1] observed that the crack growth rate is affected significantly by the change in biaxial stress field. Sunder and Ilchenko[17] performed biaxial tests on cruciform coupons by superimposing constant amplitude loading with quasi-static load, simulating cabin pressure, and computed characteristic mode I stress intensity factor (SIF) accounting for instantaneous biaxiality. Lee and Taylor[18] observed that the fatigue crack growth is faster in out-of-phase loading than in-phase loading. Misak et al[19] investigated the behaviour of 7075-T6 aluminium alloy under in-plane biaxial tension with varying biaxiality ratios and characterized the relationship between crack growth rate and energy release rate. Mall and Perel[3] performed tension-tension fatigue tests under out-of-phase loading and observed that 2 cracks initiated and propagated because of the phase difference. Meischel et al[20] quantified the influence of very high cycle fatigue on the fatigue life of Al7075 alloys using constant and variable amplitude loading. Gates and Fatemi[21] studied the effects of notches and multiaxial stress states on mode I crack growth in notched tubular and plate specimens of Al 2024-T3 alloy. They found that crack growth rates for specimens subjected to multiaxial nominal stress states were higher than those for uniaxial conditions for the same nominal mode I stress intensity factor range. Lopez-Crespo et al[22] studied the crack initiation and propagation behaviour in St52-3N steel under biaxial conditions. The crack propagation was studied using critical plane models, and it was concluded that the best predictions were obtained using the Fatemi-Socie model. Baptista et al[23] studied the fatigue crack propagation under varying phase difference using critical plane methods and concluded that none of the methods are capable of accurately predicting the crack initiation angle under phase difference. They also concluded that using a notched specimen gives consistent results compared to unnotched ones. However, to the best of author's knowledge, there is no reported literature on the study of fatigue behaviour bridging microscale phenomena to crack propagation and fatigue life under a wide range of complex in-plane biaxial loading. The currently published literature does not address the details of fracture surface morphology and the microscale damage modes that are active during fatigue crack propagation under in-plane biaxial out-of-phase fatigue loading.

In this research, extensive quasi-static and fatigue tests were conducted to study the crack initiation and propagation of Al7075-T651 cruciform specimens subjected to in-phase and out-of-phase loading conditions. Microstructural characterization was performed to understand the morphology of material microstructure and intermetallic particles. Fractography was subsequently performed on the tested specimens to understand the crack initiation and propagation behaviour, and a comprehensive analysis of the fracture surface morphology is presented. This paper is organized as follows. In Section 2, the results of microstructural material characterization are presented. Section 3 provides the details of the biaxial experimental set-up for quasi-static and fatigue tests. The results of crack growth under different loading conditions are discussed in Section 4.

2 | MATERIAL CHARACTERIZATION

Understanding the material constituents is essential for understanding crack initiation and propagation at the

microscale. The intermetallic particles are preferential sites for fatigue crack initiation, and therefore, it is necessary to study the behaviour and properties of these constituents. The second phase particles in Al7075-T6 were identified using scanning electron microscopy (SEM), and their phases and elements were identified using energy dispersive X-ray spectroscopy (EDS). An XL 30 Environmental Scanning Electron Microscope Field Emission Gun was used to perform EDS. The intermetallic particles are brittle in nature and act as crack initiation sites; therefore, their distribution and composition are studied for both healthy and fatigued samples. Polished samples (10 mm × 10 mm × 6.35 mm) were prepared from the rolled aluminium plate using a Streurs Labopol 5 polisher. Diamond suspensions of different particle sizes were used to incrementally increase the surface finish, and colloidal silica (OP-S) suspension with a particle size of 0.04 μm was used for the final polish.

The SEM micrograph and the elemental compositions of polished specimen are shown in Figure 1. Two kinds of particles were primarily observed: the Fe-bearing white particles and the Si-bearing dark particles. The Fe-bearing particles are brittle and hard with their modulus greater than the matrix material, and microcracks nucleate at these particles because of the stress concentration at their boundaries.[8]

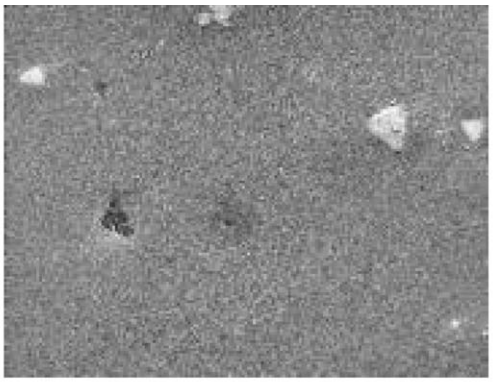

(A) SEM micrograph

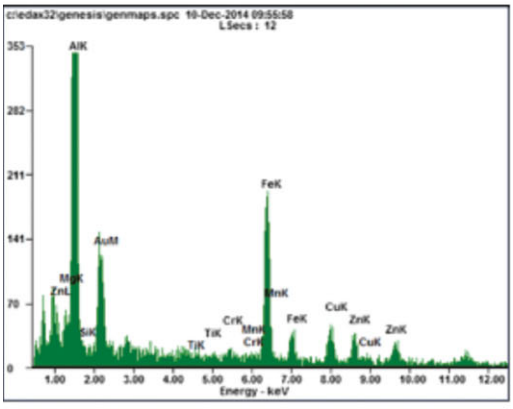

(B) Elemental composition of Fe-bearing particles

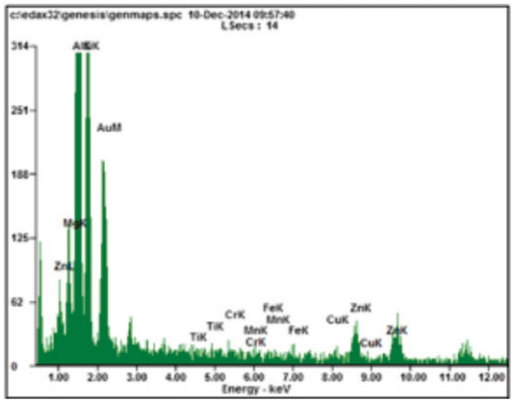

(C) Elemental composition of Si-bearing particles

FIGURE 1 Energy dispersive X-ray spectroscopy analysis showing the composition of intermetallic particles. SEM, scanning electron microscopy [Colour figure can be viewed at wileyonlinelibrary.com]

3 | BIAXIAL EXPERIMENTAL SET-UP

Quasi-static and fatigue experiments were conducted using the MTS frame with a capacity of 100 kN planar biaxial and 1100 N-m torsion and equipped with 6 independent controllers shown in Figure 2. Quasi-static experiments allow the study of plastic deformation and monotonic fracture as damage modes, whereas the fatigue experiments emphasize on crack nucleation and short crack propagation. Appropriate specimen design is essential to accurately capture the damage mechanisms associated with different loading conditions. Cruciform specimen shown in Figure 3 was designed such that the central web area had uniform stress distribution for initial yielding. The specimens were machined from 6.35-mm rolled Al7075-T651 sheets with the thickness of web area being 1.8 mm. A hole of diameter 6.35 mm was cut at the centre of the web area, and a notch of length 1.5 mm and width 0.36 mm was made at an angle of 45° (Figure 3) to accelerate crack initiation. In this fatigue study, the notch at 45° angle also facilitates the calculation of mode-mixity ratio at the crack tip when the crack initiates and propagates under out-of-phase biaxial loading. In the absence of this notch, the cracks could initiate at any arbitrary angle and direction from the periphery of the centre hole, and analysis of mode mixity on the crack tip can become challenging. Mall and Perel[3] used a similar notch design at the centre hole of a cruciform specimen to study the effect of the mode mixity in cruciform specimens on fatigue crack growth behaviour.

A high-resolution optical camera was positioned on the rear side of the specimen to capture the crack

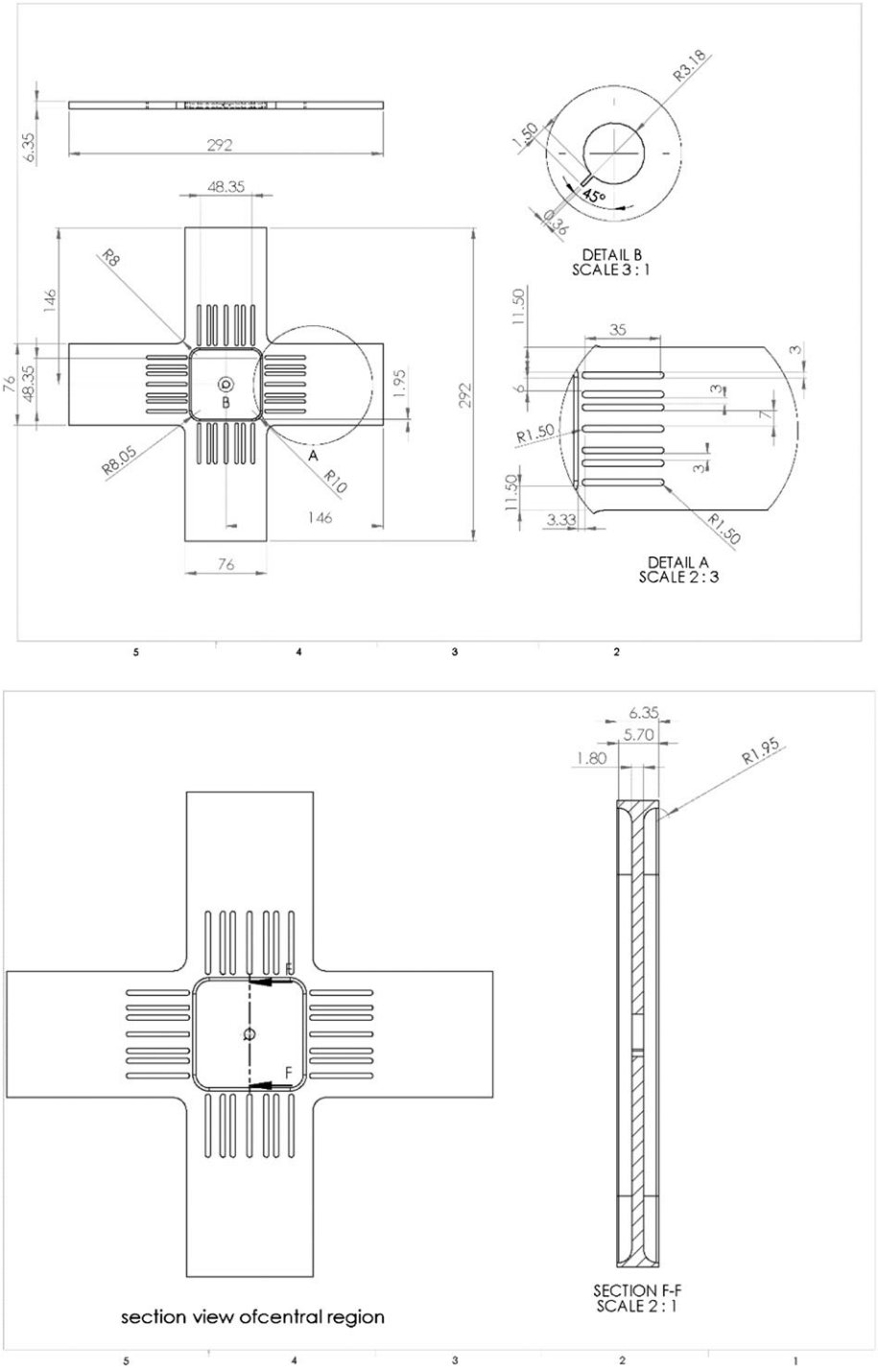

FIGURE 2 Cruciform specimen with dimensions

initiation and growth. The camera was programmed using LabVIEW to take images at a user-defined time interval. A MATLAB code was developed to convert the time stamp of the images into the number of cycles. This allowed calculating the cycles for crack initiation, propagation, and final failure. Following the fatigue tests, fractography was performed on the fatigued specimens to study the microstructural crack growth features.

4 | RESULTS AND DISCUSSION

4.1 | Quasi-static tests

Quasi-static tests were performed to obtain the loads necessary for low cycle and high cycle fatigue testing. The cruciform sample was loaded in tension up to the maximum capacity of the frame (100 kN) in both x and y

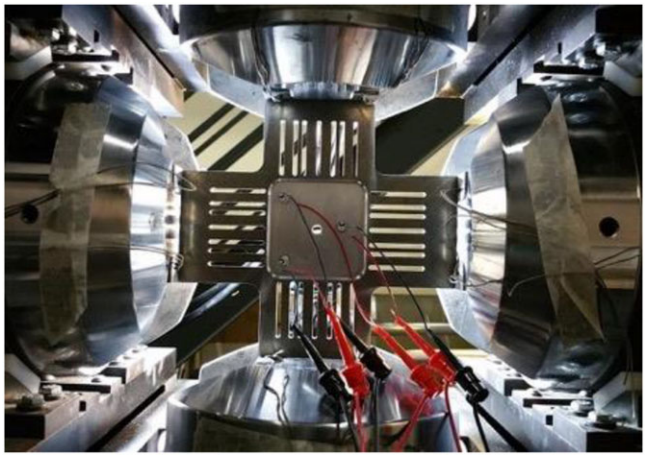

FIGURE 3 Cruciform specimen in biaxial test frame [Colour figure can be viewed at wileyonlinelibrary.com]

directions, and the tests were conducted for different values of the biaxiality ratio, BR = 0.25, 0.5, 1, 2, 4, defined as the ratio of load between x and y axes. The results are summarized in Table 1, and it can be observed that the maximum failure load was very similar for the different BR values. The failure load is defined as the load to complete fracture of the specimen. The reason can be attributed to the 45° notch angle. Since the notch is symmetric with respect to both x and y axes, the crack path remains perpendicular to the maximum loading direction and fails when the critical load is reached.

4.2 | Fatigue tests

Two cyclic load conditions with a maximum force of 15 and 30 kN for cases (i) and (ii), respectively, were selected on the basis of the results of quasi-static tests; these loads correspond to 25% and 50% of the yield stress. The load ratio for both cases was 0.1 ((i) Load1: 1.5-15 kN and (ii) Load2: 3-30 kN). When Load1 was applied along both axes, the fatigue life exceeded 75 000 cycles, and when Load2 was applied, the fatigue life was considerably shorter at approximately 11 300 cycles. Here, the fatigue life is defined as the number of cycles till the complete fracture of the specimen. These 2 loading conditions were chosen to capture the behaviour under very high and relatively low loads (low cycle and high cycle fatigue). Fatigue tests were conducted with both in-phase and out-of-phase loading. In-phase is defined such that the cyclic loading along the x and y directions is synchronized and there is no phase difference between the sinusoidal loads. For out-of-phase tests, a phase difference of 45°, 90°, and 180° was introduced. Since the fatigue life under Load2 was significantly lower, Load1 was used to perform all the experiments since it enables understanding of the necessary crack growth features. Table 2 shows the details of all the fatigue tests performed, along with the number of cycles for crack initiation and specimen failure.

TABLE 1 Static test results

Test	Biaxiality Ratio (X/Y)	Failure Load, N (X, Y)	Time to Failure, s
1	1	78 971 78 965	1211
2	0.5	90 108 45 157	1384
3	0.25	82 019 20 548	1257
4	2	39 718 79 161	1217
5	4	20 150 78 818	1240

4.2.1 | In-phase loading

For in-phase loading, a single crack initiated and propagated perpendicular to the maximum load as shown in Figure 4. A secondary crack was also observed to initiate and propagate in the opposite direction due to the stress concentrations at the opposite side of the hole created by the opening of primary crack. The results in Figure 4A,B indicate that the crack always propagates perpendicular to the maximum tangential stress. The fatigue life under these loading conditions was very similar at 10 851 and 13 971 cycles, respectively. Similarly, Figure 4C shows that the crack propagates at an angle of approximately 45° when the load is equal along horizontal and vertical directions. In all these cases, a secondary crack initiates and propagates in opposite direction because of the stress concentrations created by the opening and closing of primary crack. The fracture surface was studied for the crack shown in Figure 4C to understand the crack initiation and propagation behaviour. The crack propagation is primarily driven by the stress intensity factor range (ΔK); the fracture surface composes of 3 different morphologies with the operative mechanism dependent on ΔK.

The fracture surface of stage I crack growth (low ΔK) regime is shown in Figure 5. The highly tortuous crack path due to the crack propagation along the intense slip bands, resulting in heterogeneous deformation and tortuous crack growth, is shown in Figure 5A. The features of crystallographic facets near the crack initiation site are shown in Figure 5B, and Figure 5C shows the cracked Fe-rich intermetallic particle near the crack initiation, which indicates that the Fe-rich particles serve as the

TABLE 2 Biaxial testing under varying load conditions

Test	Load *x*	Load *y*	Frequency, Hz	Phase Difference, °	Cycles to 1-mm Crack	Cycles to Failure
1	Load2	Load2	10	0	2100	11 300
2	Load1	Load1	10	0	6000	87 087
3	Load1	Load1	15	0	6000	78 578
4	Load1	Load2	10	0	1800	13 971
5	Load2	Load1	10	0	1800	10 851
6	Load1	Load1	10	45	4500	63 000
7	Load1	Load1	10	45	5500	82 000
8	Load1	Load1	10	45	6000	76 800
9	Load1	Load1	10	90	22 800	131 800
10	Load1	Load1	10	90	16 100	135 700
11	Load1	Load1	10	90	17 400	120 600
12	Load1	Load1	10	180	18 900	75 000
13	Load1	Load1	10	180	18 300	70 000
14	Load1	Load1	10	180	11 700	60 000

Load1: 1.5-15 kN; Load2: 3-30 kN.

crack initiation sites because of their higher modulus with respect to the matrix. Cleavage facets were observed in the transition between stage I and stage II crack growth regimes, as shown in Figure 6A. The cleavage facets merge in the direction of crack growth; this information can be used to identify the crack initiation and growth events, and these facets transition into fatigue striations as shown in Figure 6B. In the stage II crack growth regime, multiple slip systems are activated, and the deformation is homogeneous. The fatigue striations (Figure 6B) are oriented perpendicular to the crack growth direction, and the spacing between the striations can be correlated with the crack growth rate. The distance between 2 striations is the crack growth per loading cycle. When the size of plastic zone exceeds the mean grain diameter, fatigue striations often extend over multiple grains.

In the fast fracture regime (stage III), a dimpled structure that is a characteristic of monotonic ductile fracture was observed. As the crack length increases, the fracture surface showed higher density of dimples resembling static ductile fracture mode. Fading striations and appearance of dimples are shown in Figure 7A, which suggests a highly ductile fracture mode. The dimples nucleate at the inclusions forming microvoids that grow and coalesce. High density of dimples was observed towards the end of stage III crack growth regime (Figure 7B) indicating static ductile fracture. It can be concluded that, in the case of in-phase loading, the crack driving force was essentially mode I in nature since the crack was observed to grow normal to the maximum tangential stress with no turning or blunting. The fractography results showing clear and uniform striation formation in stage II, heavily dimpled fracture surface in stage III, and absence of any wear/abrasion marks throughout the fracture surface also indicate a purely mode I fatigue crack growth.[24]

4.2.2 | Out-of-phase loading

Three different phase differences in loading, 45°, 90°, and 180°, were studied to understand the effect of mixed-mode fracture on the crack propagation behaviour. Under out-of-phase loading, the fatigue crack is expected to experience a mixed-mode stress state with the mode-mixity ratio, $M_R = K_{II}/K_I$, varying with the direction of the crack and the instantaneous ratio of the applied biaxial stresses. Since the notch is at 45° to the loading axis, the stress acting at the notch tip is purely mode I ($K_{II} = 0$) when in-phase loading with BR = 1 is applied. The introduction of a phase difference leads to stress components that contribute to K_{II} in addition to K_I resulting in mixed-mode stress state.[25] The influence of K_{II} increases as phase difference increases from 0° to 180°. During the out-of-phase cyclic loading, stress intensity factor becomes purely mode I at the instant when the load in *x* and *y* directions reaches the same magnitude. Subsequently, as the difference between the loads increases, K_{II} increases accordingly. The crack paths under different phase differences in loading are shown in Figure 11, and the crack formation mechanism is discussed in detail in the subsequent sections.

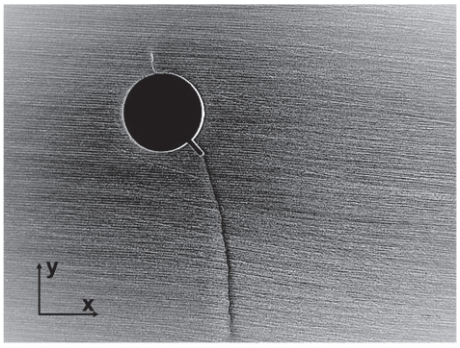

(A) Load *x*: 3-30 kN; Load *y*: 1.5-15 kN

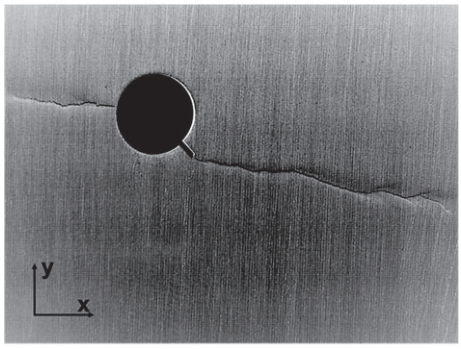

(B) Load *x*: 1.5-15 kN; Load *y*: 3-30 kN

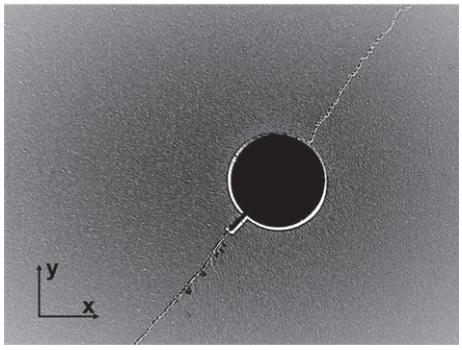

(C) Load *x*: 1.5-15 kN; Load *y*: 1.5-15 kN

FIGURE 4 Crack growth under biaxial in-phase loading

4.2.3 | Phase difference of 45°

A single crack was observed to initiate and propagate (Figure 8A) under a phase difference of 45°, and the fatigue life was similar to the specimens under in-phase loading (approximately 80 000 cycles). The plots of crack length and crack growth rate as a function of the number of cycles are shown in Figure 9. No significant change in the expected crack growth was observed with the crack growth rates in the order of 10^{-3} mm per cycle. This indicates that the contribution from K_{II} is not significant enough to affect the crack growth behaviour. During the 45° out-of-phase loading cycle, the mode-mixity ratio, M_R, varies from 0 to 0.66, and K_I remains the dominant crack driving force throughout the fatigue tests.

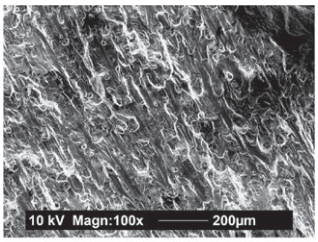

(A) Stage I morphology showing tortuous crack path (100x)

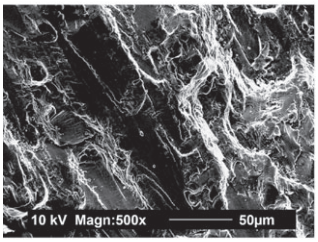

(B) Angular crystallographic facets near crack initiation (500x)

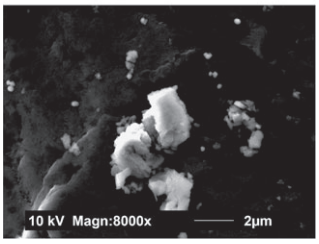

(C) Cracked Fe rich intermetallic particle near the crack initiation site (8000x)

FIGURE 5 Fracture surface in stage I crack growth regime

Fractography was performed to study the crack growth mechanism, and the results are shown in Figure 10. The near threshold regime (stage I) crack growth behaviour shown in Figure 10A indicates that pronounced intermetallic particle shearing was a dominant feature in the region of crack initiation. Transgranular cracking and faceted, crystallographic fracture mode were also observed in the crack initiation region (Figure 10B), but these features were not as prevailing as intermetallic particle fracture. Since the influence of K_{II} is not as high compared to the 90° and 180° phase difference cases and mode I remains the dominant form of fracture, lower fatigue life to crack initiation is observed compared to 90° and 180° cases, which is also reflected in the fracture features that lack angular facets and unevenness. As the crack growth approaches stage II, slip steps with superimposed fatigue striations, which indicate the influence of K_{II}, become more prominent (Figure 10C). Merati et al[26] reported the formation of similar fracture features consisting of slip steps superimposed with striations under mixed-mode fatigue fracture. Clear striations along with intermetallic particle fracture and an uneven fracture surface can be observed, which can be attributed to the mixed-mode crack growth (Figure 10D). In the stage III or the fast fracture regime, striations and slip steps start to diminish, and formation of dimples that are indicative of a static type mode I dominated tensile failure mode is observed (Figure 10E).

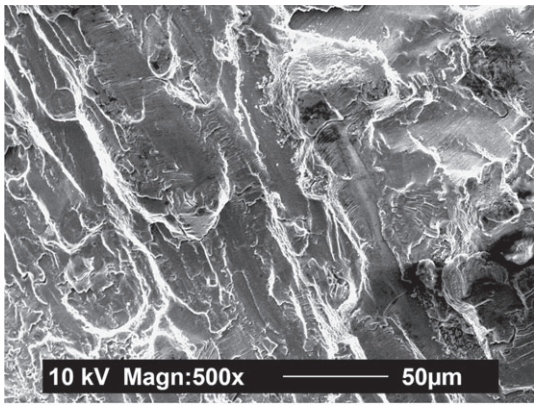

(A) Cleavage facets (500x)

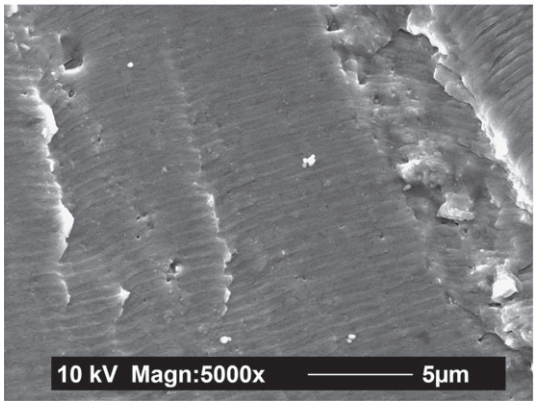

(B) Fatigue striations (5000x)

FIGURE 6 Fracture surface in stage II crack growth regime

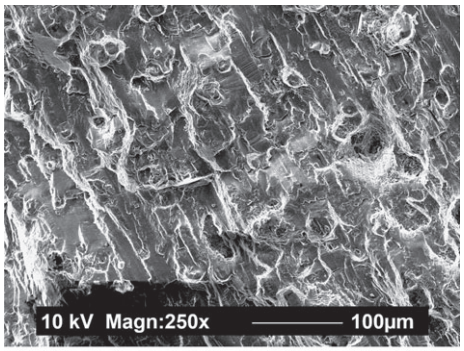

(A) Fading striations and appearance of dimples (250x)

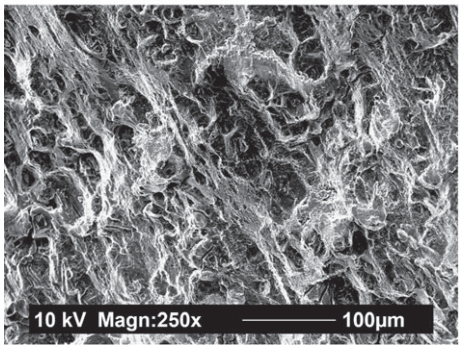

(B) High density of dimples resembling static ductile fracture (250x)

FIGURE 7 Fracture surface in stage III crack growth regime

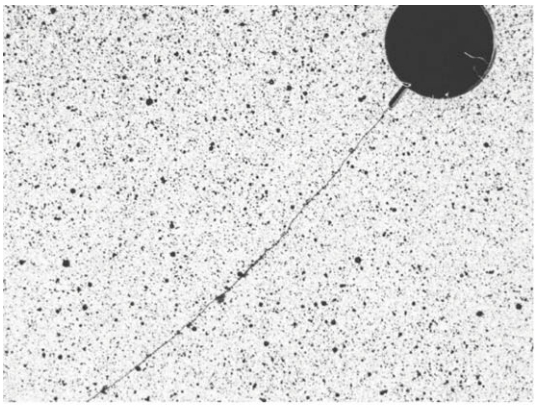

(A) Phase difference = 45°

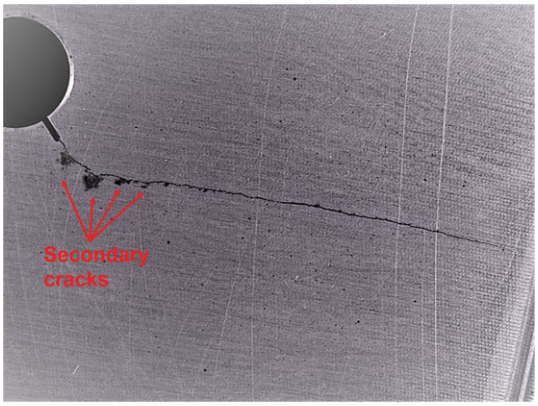

(B) Phase difference = 90°

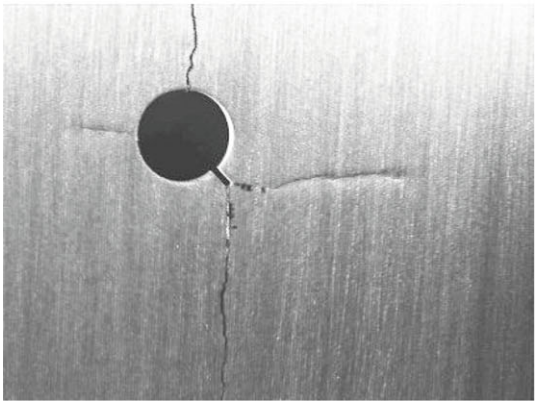

(C) Phase difference = 180°

FIGURE 8 Crack growth under biaxial out-of-phase loading [Colour figure can be viewed at wileyonlinelibrary.com]

4.2.4 | Phase difference of 90°

When the phase difference was 90°, a single crack initiated and propagated; however, the crack path was not smooth, and blunting of the crack tip along with crack arrest, which are a result of increased crack closure, can be seen in Figure 11B. The major crack tends to split into 2 cracks, but only one primary crack propagates, the direction of which is governed by the local microstructure and the mixed-mode stress state at the crack tip. During the 90° out-of-phase loading, M_R varies from 0 to 1.1;

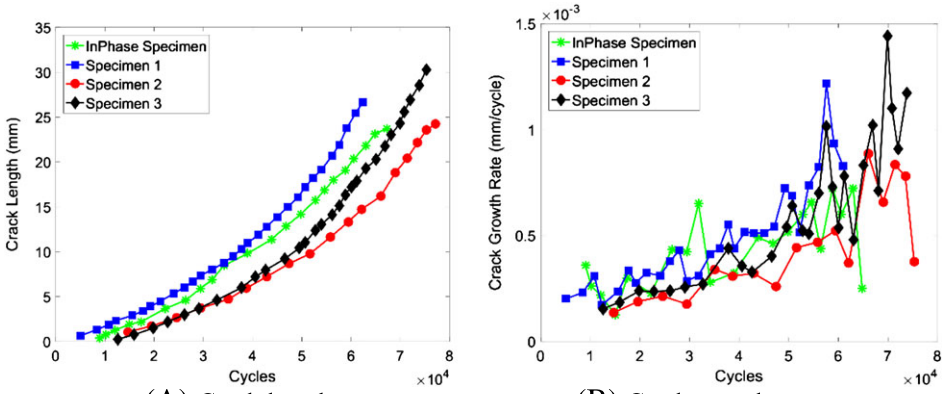

(A) Crack length (B) Crack growth rate

FIGURE 9 Fatigue crack growth under 45° phase difference [Colour figure can be viewed at wileyonlinelibrary.com]

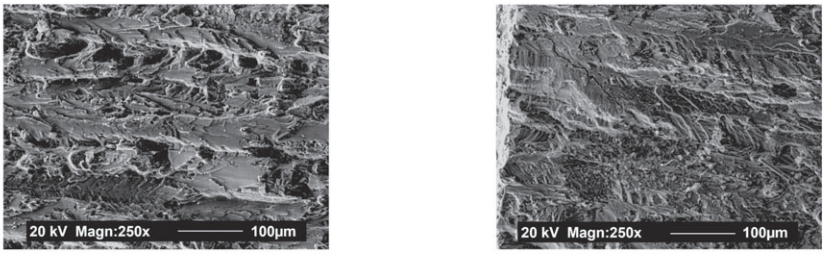

(A) Stage I crack growth; highly torturous crack path, ridges and series of fracture at intermetallic particles (250x)

(B) Transgranular cracking and faceted fracture surface (250x)

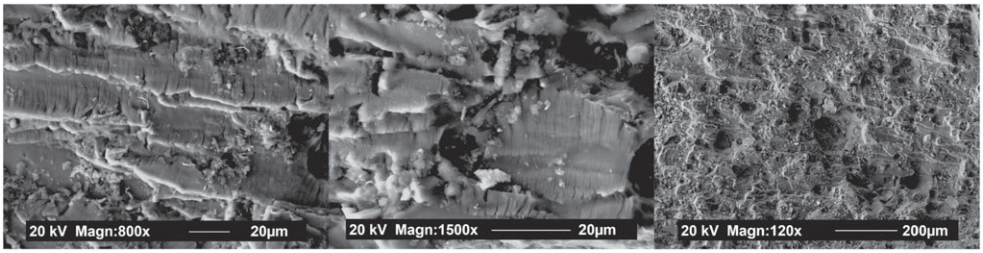

(C) Clear striations superimposed on series of slip steps (500x)

(D) Fatigue striations and sheared intermetallic particle sites on uneven fracture surface (1500x)

(E) Dimpled fracture surface due to necking around intermetallic particles (120x)

FIGURE 10 Crack growth behaviour for 45° out-of-phase loading

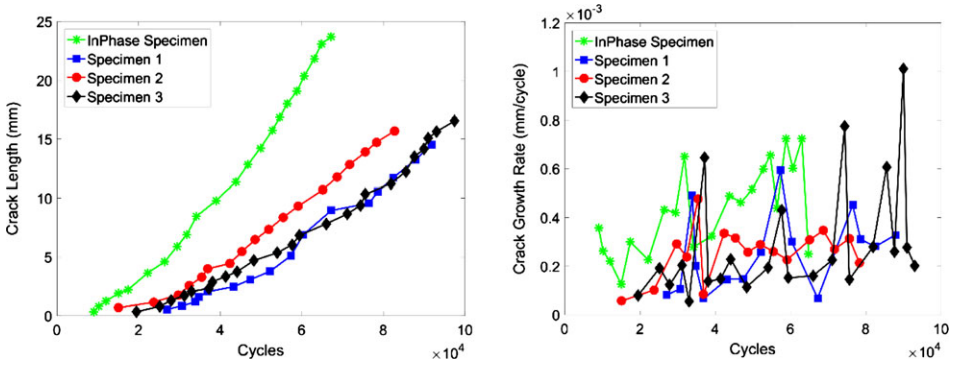

(A) Crack length (B) Crack growth rate

FIGURE 11 Fatigue crack growth under 90° phase difference [Colour figure can be viewed at wileyonlinelibrary.com]

however, for the most part, K_I remains the dominant mode with K_{II} exceeding K_I for a very short portion of the cycle. Because of the influence of K_{II}, the crack flanks slide against each other that causes increased crack closure in addition to the plasticity-induced crack closure from K_{II}. Consistent influence of K_{II} during part of each fatigue cycle results in repeated blunting and deflection of the crack tip, in turn significantly increasing the fatigue life. The plots of crack length and crack growth rate are shown in Figure 11, which indicate that the crack growth rate is significantly lower (10^{-4} mm per cycle) compared to 45° phase difference. Similar crack retardation phenomenon was observed by Sonsino[27] when a phase difference of 90° was applied under axial-torsion loading. He concluded that the crack retardation is caused by the small increase of local deformations (plastic ratcheting) when compared to in-phase loading and that the modified effective equivalent strain hypothesis delivered closest assessment to experimental results. Dahlin and Olsson[28] observed that the presence of mode II overload cycles decreases the mode I crack growth rate significantly in compact tension specimens. The mode I crack growth rate recovers only after the crack length exceeds the plastic zone generated by mode II loading. Additionally, they observed that the retardation is primarily caused due to the tangential displacement of crack surface irregularities, which induces surface mismatch between the upper and lower crack faces along with interlocking of crack asperities.

The fracture surfaces were analysed to study the crack retardation behaviour, and the microstructural features in the stage II crack growth regime are shown in Figure 12. It can be observed from Figure 12A that the crack propagation in this regime is dominated by crystallographic fracture with sharp and angular facets and a highly torturous crack path. This type of fracture surface can be attributed to the consistently competing mode I and mode II crack driving forces. The stage II crack growth regime (Figure 12B) exhibited a unique type of crack growth behaviour with negligible fatigue striations along with abrasion marks and wear debris on the fracture surface. These distinctive fracture features in stage II regime can be attributed to the significantly higher K_{II} that arises from the 90° phase difference. Since the crack path remains close to the 45° plane of the specimen, the mode II effects are more prominent. This sliding of crack faces under the influence of mode II stresses annihilates the striations, which leads to the formation of abrasion marks. The fracture feature formed near the surface of the specimen because of deflection of crack tip is shown in Figure 12C, and the splitting of crack tip is shown in Figure 12D. This was also observed in the camera image of the crack path (Figure 8B) where the crack tip tries to split and change direction at many instances, resulting in secondary microcracks and blunting of the primary crack tip. The significantly high fatigue life to failure can also be attributed to the blunting and deflection of the primary crack tip since the change in direction of the crack path results in slower crack growth rates due to the mitigation of K_I of the primary crack.

4.2.5 | Phase difference of 180°

For a phase difference of 180°, 2 cracks initiated and propagated at an angle of approximately 90° to each other as shown in Figure 8C. In addition to the 2 primary cracks, 2 secondary cracks form in exactly opposite directions similar to the in-phase loading case. The cycles to failure and crack length data (Figure 13) show that the cruciform sample fails faster with 180° phase difference (75 000) than with 90° phase difference (131 801) due to multiple crack propagation, since 2 cracks lead to a larger surface area for crack propagation. It was also observed that both the cracks propagate at the same rate (10^{-3} mm per cycle) after initiation. The secondary cracks initiated earlier compared to in-phase and out-of-phase (45° and 90°) loading because of the very high stress concentrations caused by the opening and closing of the 2 cracks.

When 180° out-of-phase loading is applied at the notch tip along the 45° plane of the specimen, the value of M_R goes from 0 to 2.17, and K_{II} becomes more dominant for a significant portion of each loading cycle. As a result, the primary crack splits into 2 cracks right after initiation. The 2 cracks then propagate symmetric to the 45° plane with an angle of 90° between them. This splitting of the crack into 2 cracks was also observed by Mall and Perel[3] for in-plane biaxial fatigue tests with 180° phase difference. The orientation of the cracks in this case can be explained using the maximum hoop stress theory,[14] which states that the crack tends to propagate in the direction that results in maximum hoop stress at the crack tip, leading to minimization of the K_{II} component of the crack driving force.

$$\theta = 2\arctan\left(\frac{1-\sqrt{1+8\left(\frac{K_{II}}{K_I}\right)^2}}{4\frac{K_{II}}{K_I}}\right). \quad (1)$$

The fracture surfaces were studied for both the cracks and were found to have similar features; therefore, the fracture surfaces are presented for one of the cracks. In stage II regime, fatigue striations were observed along multiple slip planes. Unlike in-phase loading where the deformation behaviour in stage II was homogenous, uneven striations were observed for 180° phase difference.

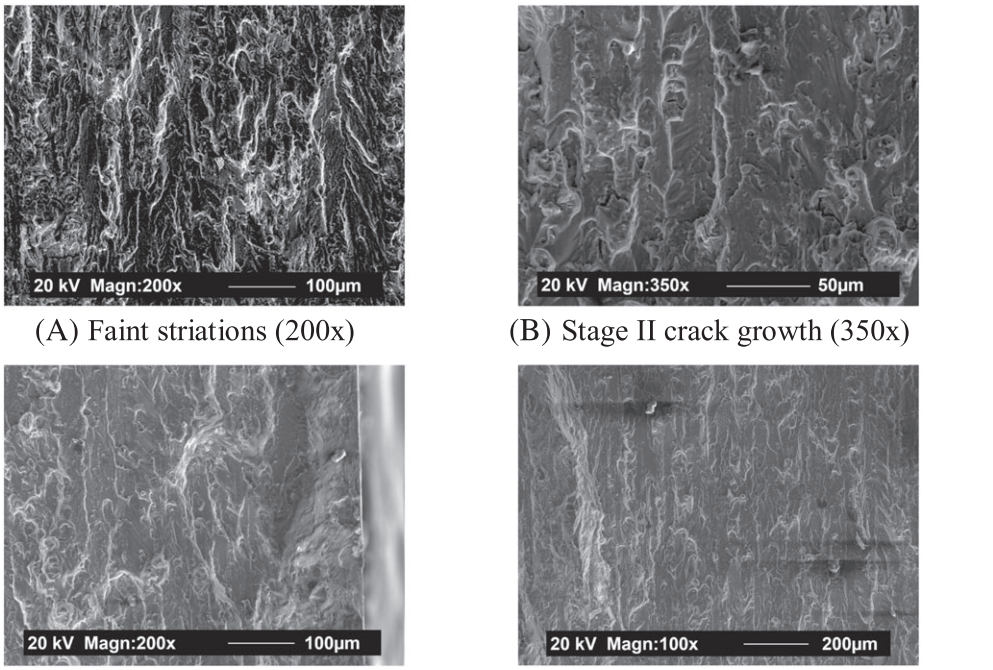

(A) Faint striations (200x) (B) Stage II crack growth (350x)

(C) Crack deflection (200x) (D) Crack tip splitting due to phase difference (100x)

FIGURE 12 Crack growth behaviour for 90° out-of-phase loading

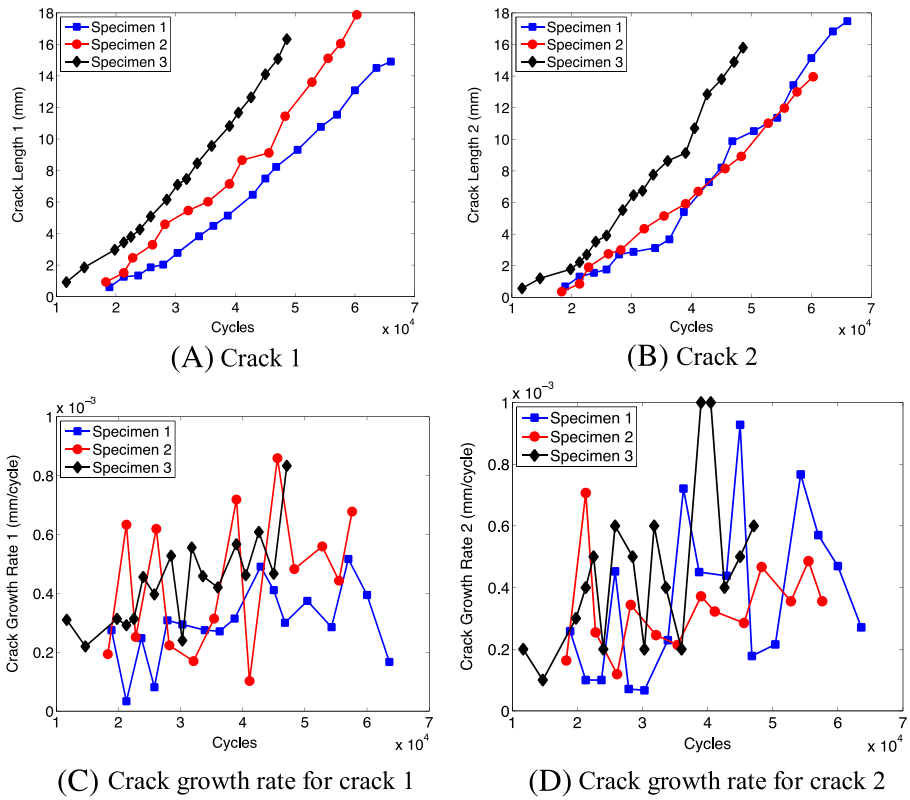

(A) Crack 1 (B) Crack 2

(C) Crack growth rate for crack 1 (D) Crack growth rate for crack 2

FIGURE 13 Fatigue crack growth under 180° phase difference [Colour figure can be viewed at wileyonlinelibrary.com]

The morphology of the crack growth with highly angular facets and fatigue striations is shown in Figure 14A. Because of the phase difference, the crack experiences mixed-mode fracture and exhibits slip steps along with fatigue striations[26] as shown in Figure 14B. The superimposition of fatigue striations and slip steps indicates

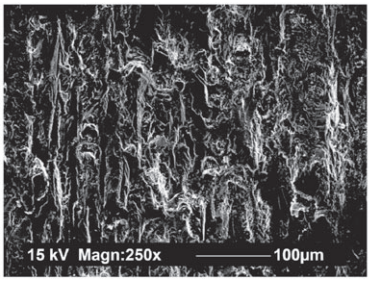

(A) Morphology of stage II crack growth regime showing highly angular facets and fatigue striations (250x)

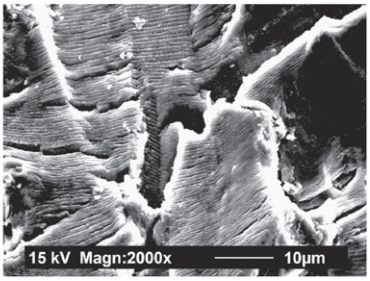

(B) Fatigue striations and slip steps superimposed on each other (2000x)

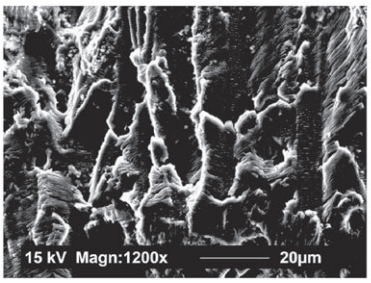

(C) Highly angular fatigue striations (1200x)

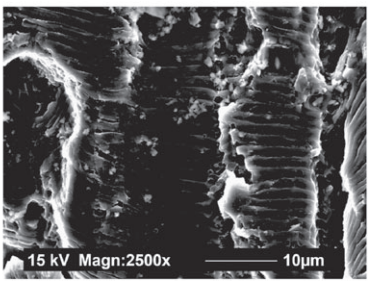

(D) Large striation spacing towards end of stage-II (2500x)

FIGURE 14 Stage II crack growth regime for crack 1

highly mixed-mode fracture at the crack tip. Uneven striations along multiple crystallographic orientations with slip steps, narrow and fine striations superimposed on each other are shown in Figure 14C. It was observed that the stage II crack growth regime lasted much longer than in case of in-phase loading.

Fractography results for the in-phase and out-of-phase biaxial fatigue tests revealed the characteristic microscale mechanisms that govern crack initiation and propagation under the different loading conditions. Distinctive fracture features in out-of-phase loading, such as slip steps with superimposed striations, wear debris, crack deflection, and crack splitting, were observed, and valuable insight was gained on the effect of out-of-phase loading on crack growth rates.

5 | CONCLUSIONS

Extensive biaxial quasi-static and fatigue tests were performed to study the crack initiation and propagation behaviour under nonproportional, in-phase, and out-of-phase loading conditions. It was observed that a single crack that initiates and propagates under in-phase loading splits into 2 cracks under out-of-phase loading with a phase difference of 180°. For phase difference of 90°, significant crack retardation was observed because of mode II–induced plasticity and plastic ratcheting of the crack tip because of the presence of mode II loading. For a phase difference of 45°, no significant change in fatigue life was observed since the contribution of mode II–induced plasticity is very low. A comprehensive microstructural characterization was performed to study the crack initiation and propagation behaviour. The SEM was used to identify the second phase intermetallic particles, and EDS was performed to identify their constituent elements. Two types of intermetallic particles were identified: (1) Fe bearing (hard) and (2) Si bearing (soft). Fractography was performed on the fracture surface, and it revealed that the cracks initiate near the hard Fe-bearing particles. Nucleation dimples were observed around the hard Fe-bearing particles in stage I crack growth regime. Fatigue striations superimposed on slip steps were observed in stage II crack growth regime, indicating highly mixed-mode fracture. The stage III crack growth regime showed large density of dimples resembling static ductile fracture. The fracture surface morphology was highly complex for out-of-phase loading (180°). Although both the cracks showed similar fractographic features, they were highly angular and complex and showed significant mixed-mode fracture features. For 45° out-of-phase loading condition, intermetallic particle fracture and consistent slip steps superimposed with striations were observed throughout the fracture surface, whereas 90° out-of-phase specimen showed almost negligible striations and signs of crack deflection that resulted

in reduced crack growth rates. The initiation and propagation of cracks in unnotched specimens will be studied in the future.

ACKNOWLEDGEMENTS

This research was sponsored by the US Navy Naval Air Systems Command and Technical Data Analysis, Inc, subcontract no. N08-006 phase III DO 0005, program manager Dr Nagaraja Iyyer.

ORCID

R.K. Neerukatti http://orcid.org/0000-0003-0337-692X

REFERENCES

1. Anderson PRG, Garrett GG. Fatigue crack growth rate variations in biaxial stress fields. *Int J Fract*. 1980;16:R111-R116.
2. Hopper C, Miller K. Fatigue crack propagation in biaxial stress fields. *J Strain Anal Eng Des*. 1977;12:23-28.
3. Mall S, Perel VY. Crack growth behavior under biaxial fatigue with phase difference. *Int J Fatigue*. 2015;74:166-172.
4. Gudlur P, Boczek A, Radovic M, Muliana A. On characterizing the mechanical properties of aluminum–alumina composites. *Mater Sci Eng A*. 2014;590:352-359.
5. Haque MA, A Saif MT (2002) Mechanical behavior of 30–50 nm thick aluminum films under uniaxial tension. *Scr Mater* 47: 863–867.
6. Oh H-K. Characterization of dynamic fatigue life by the uniaxial tensile test. *J Mater Process Technol*. 1995;54:365-371.
7. Stanzl-Tschegg S. Fatigue crack growth and thresholds at ultrasonic frequencies. *Int J Fatigue*. 2006;28:1456-1464.
8. Xue Y, El Kadiri H, Horstemeyer MF, Jordon JB, Weiland H. Micromechanisms of multistage fatigue crack growth in a high-strength aluminum alloy. *Acta Mater*. 2007;55:1975-1984.
9. Bannantine JA, Comer J, Handrock J (1990) *Fundamentals of Metal Fatigue Analysis*. 1990. Englewood Cliffs, NJ: Prentice-Hall contact. 480: 567.
10. Gdoutos E, Zacharopoulos D. A damage model for crack initiation and growth. *Theor Appl Fract Mech*. 1990;14:117-122.
11. Socie DF, Waill LA, Dittmer DF (1985) Biaxial fatigue of Inconel 718 including mean stress effects. *Multiaxial Fatigue: A Symposium*. ASTM International, STP853-EB.
12. Bennett V, McDowell D. Cyclic crystal plasticity analyses of stationary, microstructurally small surface cracks in ductile single phase polycrystals. *Fatigue Fract Eng Mater Struct*. 2002;25:677-693.
13. Zhang J, Liu K, Chattopadhyay A (2012) Fatigue life prediction under biaxial FALSTAFF loading using statistical volume element based multiscale modeling. ASME 2012 International Mechanical Engineering Congress and Exposition. American Society of Mechanical Engineers, 625–634.
14. Erdogan F, Sih G. On the crack extension in plates under plane loading and transverse shear. *J Basic Eng*. 1963;85:519-527.
15. Sih GC. Strain-energy-density factor applied to mixed mode crack problems. *Int J Fract*. 1974;10:305-321.
16. Hallbäck N, Nilsson F. Mixed-mode I/II fracture behaviour of an aluminium alloy. *J Mech Phys Solids*. 1994;42:1345-1374.
17. Sunder R, Ilchenko B. Fatigue crack growth under flight spectrum loading with superposed biaxial loading due to fuselage cabin pressure. *Int J Fatigue*. 2011;33:1101-1110.
18. Lee E, Taylor R. Fatigue behavior of aluminum alloys under biaxial loading. *Eng Fract Mech*. 2011;78:1555-1564.
19. Misak H, Perel V, Sabelkin V, Mall S. Crack growth behavior of 7075-T6 under biaxial tension–tension fatigue. *Int J Fatigue*. 2013;55:158-165.
20. Meischel M, Stanzl-Tschegg S, Arcari A, Iyyer N, Apetre N, Phan N. Constant and variable-amplitude loading of aluminum alloy 7075 in the VHCF regime. *Procedia Eng*. 2015;101:501-508.
21. Gates N, Fatemi A. Fatigue crack growth behavior in the presence of notches and multiaxial nominal stress states. *Eng Fract Mech*. 2016;165:24-38.
22. Lopez-Crespo P, Moreno B, Lopez-Moreno A, Zapatero J. Study of crack orientation and fatigue life prediction in biaxial fatigue with critical plane models. *Eng Fract Mech*. 2015;136:115-130.
23. Baptista R, Cláudio R, Reis L, Madeira J, Freitas M. Numerical study of in-plane biaxial fatigue crack growth with different phase shift angle loadings on optimal specimen geometries. *Theor Appl Fract Mech*. 2016;85:16-25.
24. Wanhill RJ. Fractography of fatigue crack propagation in 2024-T3 and 7075-16 aluminum alloys in air and vacuum. *Metall Mater Trans A*. 1975;6:1587-1596.
25. Buchholz F-G, Chergui A, Richard H. Fracture analyses and experimental results of crack growth under general mixed mode loading conditions. *Eng Fract Mech*. 2004;71:455-468.
26. Merati A, Hellier A, Zarrabi K. On the mixed mode II/III fatigue threshold behaviour for aluminium alloys 2014-T6 and 7075-T6. *Fatigue Fract Eng Mater Struct*. 2012;35:2-12.
27. Sonsino C. Influence of load and deformation-controlled multiaxial tests on fatigue life to crack initiation. *Int J Fatigue*. 2001;23:159-167.
28. Dahlin P, Olsson M. Mode I fatigue crack growth reduction mechanisms after a single mode II load cycle. *Eng Fract Mech*. 2006;73:1833-1848.

How to cite this article: Neerukatti RK, Datta S, Chattopadhyay A, Iyyer N, Phan N. Fatigue crack propagation under in-phase and out-of-phase biaxial loading. *Fatigue Fract Eng Mater Struct*. 2018;41:387–399. https://doi.org/10.1111/ffe.12690